Biodistribution and Radiation Dosimetry of LMI1195: First-in-Human Study of a Novel ^{18}F-Labeled Tracer for Imaging Myocardial Innervation

Albert J. Sinusas[1,2], Joel Lazewatsky[3], Jacqueline Brunetti[4], Gary Heller[5], Ajay Srivastava[1], Yi-Hwa Liu[1], Richard Sparks[6], Andrey Puretskiy[6], Shu-fei Lin[2], Paul Crane[3], Richard E. Carson[2], and L. Veronica Lee[3]

[1]Section of Cardiovascular Medicine, Department of Medicine, Yale University School of Medicine, New Haven, Connecticut; [2]Department of Diagnostic Radiology, Yale University School of Medicine, New Haven, Connecticut; [3]Lantheus Medical Imaging, North Billerica, Massachusetts; [4]Holy Name Medical Center, Teaneck, New Jersey; [5]Morristown Medical Center, Morristown, New Jersey; and [6]CDE Dosimetry Services, Knoxville, Tennessee

A novel ^{18}F-labeled ligand for the norepinephrine transporter (*N*-[3-bromo-4-(3-^{18}F-fluoro-propoxy)-benzyl]-guanidine [LMI1195]) is in clinical development for mapping cardiac nerve terminals in vivo using PET. Human safety, whole-organ biodistribution, and radiation dosimetry of LMI1195 were evaluated in a phase 1 clinical trial. **Methods:** Twelve healthy subjects at 3 clinical sites were injected intravenously with 150–250 MBq of LMI1195. Dynamic PET images were obtained over the heart for 10 min, followed by sequential whole-body images for approximately 5 h. Blood samples were obtained, and heart rate, electrocardiogram, and blood pressure were monitored before and during imaging. Residence times were determined from multiexponential regression of organ region-of-interest data normalized by administered activity (AA). Radiation dose estimates were calculated using OLINDA/EXM. Myocardial, lung, liver, and blood-pool standardized uptake values were determined at different time intervals. **Results:** No adverse events due to LMI1195 were seen. Blood radioactivity cleared quickly, whereas myocardial uptake remained stable and uniform throughout the heart over 4 h. Liver and lung activity cleared relatively rapidly, providing favorable target-to-background ratios for cardiac imaging. The urinary bladder demonstrated the largest peak uptake (18.3% AA), followed by the liver (15.5% AA). The mean effective dose was 0.026 ± 0.0012 mSv/MBq. Approximately 1.6% AA was seen in the myocardium initially, remaining above 1.5% AA (decay-corrected) through 4 h after injection. The myocardium-to-liver ratio was approximately unity initially, increasing to more than 2 at 4 h. **Conclusion:** These preliminary data suggest that LMI1195 is well tolerated and yields a radiation dose comparable to that of other commonly used PET radiopharmaceuticals. The kinetics of myocardial and adjacent organ activity suggest that cardiac imaging should be possible with acceptable patient radiation dose.

Key Words: sympathetic imaging; positron emission tomography; dosimetry; biodistribution; myocardium

J Nucl Med 2014; 55:1445–1451
DOI: 10.2967/jnumed.114.140137

Received Mar. 9, 2014; revision accepted May 13, 2014.
For correspondence or reprints contact: Albert J. Sinusas, Department of Medicine, Yale University School of Medicine, 789 Howard Ave., DANA 3, P.O. Box 208017, New Haven, CT 06510-8017.
E-mail: albert.sinusas@yale.edu
Published online Jul. 3, 2014.

Heart failure (HF) is a growing health problem in the United States, affecting more than 5.3 million people in 2005 (*1,2*), and patients with HF are 6–9 times more likely to have sudden cardiac death (SCD), compared with the rate of the general population. HF and SCD are associated with abnormalities of the cardiac sympathetic function.

Alterations in cardiac sympathetic function occur early in the development of HF, even before the augmented sympathetic outflow to other organs (*3*). These changes include increased norepinephrine release from cardiac sympathetic nerves and decreased cardiac norepinephrine reuptake (*4*), which lead to elevated cardiac sympathetic tone. The cardiac neuronal norepinephrine transporter (NET) is mainly responsible for norepinephrine clearance at the synaptic cleft. Impaired function of NET in HF has been identified in the hearts of humans with diverse etiologies, including hypertension, valvular and ischemic heart disease, and idiopathic hypertrophic cardiomyopathy (*4–7*). Thus, measuring NET function may be a useful target for monitoring the development and likelihood of progression of HF and for assessing risk for SCD. Nuclear cardiac imaging provides a unique tool to measure the molecular changes in the heart, including cardiac function of NET, in a noninvasive and repeatable manner (*8*).

Currently, ^{123}I-metaiodobenzylguanidine (^{123}I-MIBG), an iodinated neurotransmitter analog, is commonly used for SPECT imaging of sympathetic function of the heart in Japan and Europe (*8,9*) and was recently approved for cardiac sympathetic imaging in the United States. The neuronal uptake of ^{123}I-MIBG in the heart is primarily by the NET, via an energy-dependent uptake 1 mechanism that is sensitive to desipramine inhibition (*10*). In the past 2 decades, many studies have demonstrated that cardiac uptake of ^{123}I-MIBG is lower in individuals with HF (*8,9*). Furthermore, patients with the lowest uptake, as reflected by the heart-to-mediastinal ratio, or with the fastest washout from the heart tend have the poorest prognosis (*8,9*). Multiple studies suggest that ^{123}I-MIBG can be used as an independent predictor of HF progression and cardiac mortality (*11–13*).

^{11}C-metahydroxyephedrine is another NET ligand that has been used for PET imaging of cardiac sympathetic function. However, widespread clinical imaging with this agent has been limited by the short half-life (~20 min) of ^{11}C and the need for an on-site cyclotron. A recently completed single-site prospective study

(Prediction of ARrhythmic Events With Positron Emission Tomography [PAREPET]; NCT01400334) of coronary artery disease patients who were candidates for an implantable cardiovertor defibrillator placement for primary prevention of SCD applied ^{11}C-metahydroxyephedrine PET imaging and demonstrated that the extent of denervation assessed with quantitative PET was one of the best predictors of SCD (*14*).

N-[3-bromo-4-(3-^{18}F-fluoro-propoxy)-benzyl]-guanidine (LMI1195) is another novel PET imaging agent developed for evaluation of sympathetic neuronal function in the heart (*15*). This agent is a benzylguanidine analog, in the same class as MIBG, but labeled with ^{18}F, a positron emitter having a significantly longer half-life (~110 min) than ^{11}C. LMI1195 could potentially improve the clinical feasibility of PET sympathetic imaging and take advantage of the improved resolution and quantitative capability of PET (*15*). Yu et al. recently demonstrated that the uptake of LMI1195 was NET-mediated in both rabbits and nonhuman primates and was decreased in rodent models of HF. PET imaging studies in nonhuman primates with LMI1195 showed a favorable heart-to-liver ratio, compared with ^{123}I-MIBG (*15*).

We now report the initial first-in-human results of a multicenter single-dose phase I study evaluating the dosimetry, biodistribution, and safety of LMI1195 PET imaging in 12 young, healthy subjects at 3 sites in the United States. This report demonstrates the safety and tolerability of LMI1195 and establishes image quality as well as the whole-organ biodistribution and dosimetry. The regional variation of myocardial uptake and myocardial clearance was also evaluated in a subset of the healthy human volunteers for determination of the normal myocardial distribution.

MATERIALS AND METHODS

Study Design

We performed a multicenter phase I, nonrandomized, single-dose, open-label first-in-human study that enrolled 12 healthy subjects at 3 study centers in the United States. The study was approved by the Institutional Review Board (IRB) at each site, and each subject signed the IRB-approved, written informed consent form. The study population consisted of healthy volunteers of either sex between the ages of 18 and 40 y, with a body mass index of 18–30 kg/m^2, without significant or chronic medical illness, pregnancy, smoking within 1 mo of enrollment, or the use of any prescription drugs within 4 wk before dosing.

Subjects underwent screening procedures within 2 d before enrollment to confirm eligibility and underwent baseline procedures on the day of imaging. Subjects received a single intravenous bolus injection of 148–222 MBq (4–6 mCi) of ^{18}F-labeled LMI1195 and underwent whole-body PET imaging. The first 3 subjects were enrolled sequentially until all safety follow-up was completed on days 5–7.

Evaluation of Patient Safety

Safety was assessed at various time points by monitoring adverse events (AEs), clinical laboratory tests, electrocardiograms, physical examination, and vital signs. Subjects were confined at the study center 1 d before administration of LMI1195 (day 1) and remained confined until completion of the day 2 safety assessments. Subjects were contacted by telephone approximately 48 ± 8 h (day 3) after LMI1195 administration, for AE monitoring. Subjects returned to the study center approximately 1 wk (5–7 d) after LMI1195 administration for a follow-up safety visit, and they were contacted by telephone approximately 14–17 d after LMI1195 administration for serious-AE monitoring.

Heart rate, electrocardiograms, blood pressure, and laboratory assessments were obtained before and during imaging and at the time of the day 2 and days 5–7 follow-up evaluation and physical examination.

Laboratory Testing for Toxicity

Blood and urine sampling was performed at the time of screening, at baseline (within 2 h before LMI1195 administration), and at multiple time points up to 48 h after administration to evaluate for potential toxicity of LMI1195 and included assessment of renal and hepatic function.

PET Image Acquisition and Reconstruction Protocol

Serial whole-body PET scans were acquired in 2-dimensional mode using either a PET-only scanner (HR+; Siemens) or a PET/CT scanner (Discovery LS4 PET/CT; GE Healthcare). The supplemental data (available at http://jnm.snmjournals.org) provide details regarding our acquisition and reconstruction protocols.

Assessment of Biodistribution and Uptake and Clearance Pharmacokinetics

Venous blood and urine sampling was performed at baseline (within 2 h before LMI1195 administration) and at time points up to 8 h after administration to evaluate the pharmacokinetics of LMI1195 and ^{18}F activity and to obtain a metabolite profile in 6 subjects at the 1 clinical study center of the 3 participating that was capable of conducting the assessments. Plasma samples collected at 1, 2, 5, 15, 30, 60, 90, 120, and 240 min after injection mixed with urea at a final concentration 8 M, and selected urine samples were subjected to column-switching radio-high performance liquid chromatography (HPLC) analysis for separation of LMI1195 parent from its ^{18}F metabolites, based on a modified method published by Hilton et al. (*16*). Up to 5 mL of plasma filtrate were coinjected with synthetic unlabeled LMI1195 and metabolites to the automatic HPLC system, which consisted of an analytic mobile phase designated at 27.5% of acetonitrile in 0.1 M ammonium formate, pH 4.2, at 1.37 mL/min, with a Luna C18 (*2*) analytic column (250 × 4.6 mm, 5 μm; Phenomenex). The LMI1195 parent compound retention was 15 min. Synthetic external standards for LMI1195 parent and known metabolites had been observed during in vitro and in vivo nonclinical studies. Quantification of ^{18}F radioactivity in the HPLC eluate was fraction-collected in a timely manner and performed by a γ-counter assay.

Summary statistics were calculated for the pharmacokinetic parameters, such as maximum concentration, time of maximum concentration, elimination half-life, clearance at steady state, steady-state volume of distribution, and area under the concentration–time curve from time 0 to time t for LMI1195 and ^{18}F radioactivity in blood.

Estimation of Dosimetry

Estimates of organ absorbed doses were calculated on the basis of multiple whole-body PET images acquired at scheduled time points after administration of LMI1195 to evaluate organ, blood, and whole-body distribution. The full details of this dosimetry analysis are available in the supplemental data. For 6 of the subjects (from 2 sites) whose data were acquired on systems not capable of full whole-body imaging, images of the legs were used to estimate activity not in the field of view in the head to mid-thigh images.

Image data acquisition and dosimetry calculations were performed in accordance with the recommendations of the MIRD Committee (*17*). OLINDA/EXM software (*18*) was used to estimate organ-absorbed doses in accordance with guidelines of the U.S. Food and Drug Administration pertaining to dosimetry for experimental radiopharmaceuticals (*19*). Estimates of the effective dose (ED) equivalent and the ED were based on International Commission on Radiological Protection (ICRP) publications 26 (*20*) and 60 (*21*), respectively.

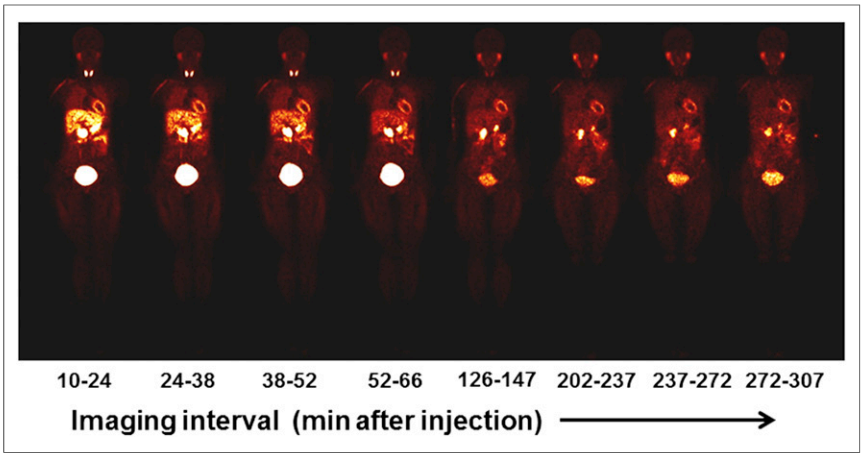

FIGURE 1. Representative sequence of whole-body LMI1195 coronal images at mid-myocardial level in human volunteer. Each whole-body image is scaled to maximum value within that image.

Regions of interest were constructed using the coronal slices to determine whole-organ activity. Image quantification was performed in general concordance with the methodology described in MIRD pamphlet no. 16 (*17*). Organ activity values were normalized where necessary to ensure that activity was conserved.

For each patient and organ, voxel sum data in the resulting volumes of interest were subjected to nonlinear least-squares regression analysis using sums of exponentials. Urinary excretion for dosimetry purposes was estimated on the basis of the total body radioactivity, quantified from the images.

The residence times (τ) were determined by integration of the resultant exponential functions. The remainder of the body τ was determined by subtraction of the organ τ from the whole-body τ. Urinary bladder τ were determined using the parameters determined by fitting the whole-body activity data with a urinary bladder model as implemented in the OLINDA/EXM software (version 1.1) (*18*), with a 3.5-h bladder-voiding interval. Red marrow τ was determined on the basis of a volume of interest created for a portion of the lumbar spine. The total lumbar spine was assumed to contain 16.1% (*22*) of the total red marrow. Absorbed dose estimates for all target organs were determined with OLINDA/EXM using the hermaphroditic adult male phantom. Salivary gland self-dose was determined using a conservative estimate of the S value for salivary glands based on the reference man total mass of the parotid and submaxillary salivary glands (*23*) and assuming a spheric shape. Final salivary gland dose estimates were determined using these S values as described in the MIRD Primer (*24*).

Global Standardized Uptake Values (SUVs) of Myocardium-to-Lung and Myocardium-to-Liver Ratios and Normal Pattern of Regional Myocardial Uptake of LMI1195

Global SUVs for the heart, liver, and lung were calculated for all subjects over the imaging period using AMIDE (*25*) and the myocardium-to-lung and myocardium-to-liver ratios calculated.

A subset of the healthy subjects ($n = 6$) from 1 of the study centers had additional analyses performed using customized cardiac analysis software (WLCQ; Medx) to establish the normal regional variation of myocardial uptake. Attenuation-corrected images at 20 min and 1 h were reoriented into standard cardiac specific axes, and regional SUVs were quantified on a sector-by-sector basis with correction for injected dose and subject weight, using the PET quantification software. Circumferential profiles were generated of the SUVs. The left ventricle was then divided into 3 short-axis slices (base, mid, apical) and each slice then divided into 4 radial sectors (anterior, septal, inferior, lateral), and mean regional SUV for each sector was calculated.

Statistical Methods

Statistical analyses and summary tables and listings were prepared using SAS (release 9.1.3 or 9.2; SAS Institute, Inc.). Standard descriptive summaries included the number of subjects, mean, median, SD, minimum, and maximum for quantitative variables; frequencies and percentages were provided for qualitative variables. Listings were sorted by subject number and time relative to dose or visit, where appropriate. Statistical comparison tests, if performed, were based on 5% level of significance.

The subjects' demographics and baseline characteristics were listed and summarized using standard descriptive statistics. The demographic profile, including age, sex, race, ethnicity, height, weight, and body mass index, were summarized for all enrolled subjects. Medical history data were collected and listed by body system in all enrolled subjects.

RESULTS

All 12 subjects who were enrolled into the trial received LMI1195 and completed the trial. The mean age ± SD of subjects was 27.8 ± 6.5 y. Most subjects were male (66.7%), not Hispanic (83.3%), and White (66.7%). The mean body mass index ± SD for subjects was 24.6 ± 3.4 kg/m^2, from a minimum of 18.9 to a maximum of 29.7 kg/m^2.

Subjects were administered a mean (±SD) dose of 1.77 ± 0.46 μg of LMI1195, from a minimum of 0.94 to a maximum of 2.76 μg of LMI1195. The average amount of ^{18}F injected was 193.5 ± 37.4 MBq (5.23 ± 1.01 mCi).

Patient Safety

There were no deaths, serious AEs, discontinuations due to AEs, or other significant AEs reported during the conduct of this trial. Five (41.7%) subjects experienced at least 1 AE; all were mild or moderate in severity. The most common AE was back pain, which was reported in 2 (16.7%) subjects, and can most likely be attributed to the long imaging times. The other AEs (1 subject, 8.3% for each) were muscle spasms, musculoskeletal discomfort, feeling hot, caffeine withdrawal headache, and micturition urgency.

There were no clinically significant laboratory results identified after injection of LMI1195. No clinically significant changes in vital signs from baseline values were identified after LMI1195 administration, and all values returned to predose levels by the end of vital sign monitoring. No clinically significant abnormalities were identified on 12-lead electrocardiography during initial review by the principal investigator at each site or by the sponsor on secondary review.

Biodistribution and Uptake and Clearance Pharmacokinetics

The radiotracer cleared quickly from the blood and demonstrated a favorable biodistribution for early cardiac imaging. A representative series of whole-body LMI1195 coronal images at the mid-myocardial level in 1 of the human volunteers acquired over the 5 h after injection is illustrated in Figure 1. The observed time–activity curves in whole organs are summarized in Figure 2. The organ with the largest peak uptake was the urinary bladder (18.3%

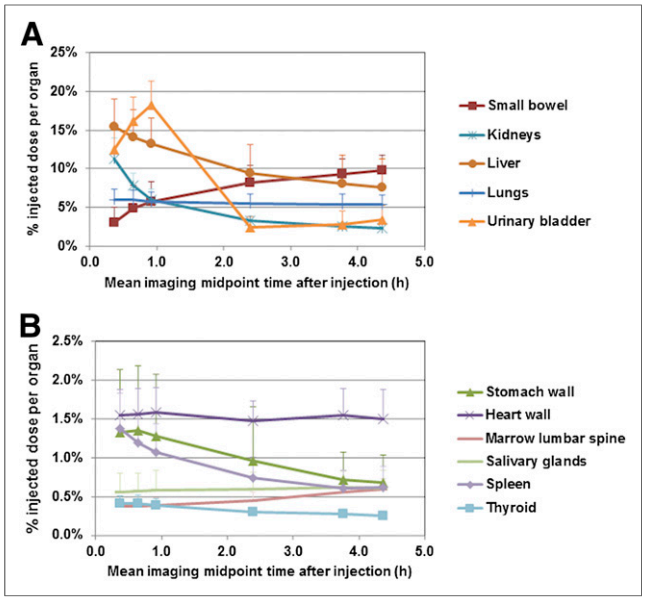

FIGURE 2. Whole-organ biodistribution of ^{18}F-LMI1195 for all source organs except whole body (expressed as percentage injected dose per organ) from approximately 10-min starting time to approximately 4.5 h. (A) Values for small bowel, kidneys, liver, lungs, and urinary bladder are illustrated. (B) Values for stomach wall, heart wall, marrow lumbar spine, salivary glands, spleen, and thyroid are illustrated. Values shown have been corrected for ^{18}F radioactive decay. Error bars represent SD.

of the injected activity at ~60 min postdose), followed by the liver (15.5% AA at ~17 min postdose). Concentrations of LMI1195 that were observed in the liver were unlikely to affect the assessment of myocardial disease in most cases. These data are summarized in Figure 2. The values reported represent the fraction of the injected radioactivity in the whole organ and not the concentration of radioactivity in the organ. Thus, these values do not necessarily reflect the relative intensity of the image in the corresponding organ, because image intensity is a function of the concentration of radioactivity rather than total radioactivity.

LMI1195 was rapidly cleared from circulation, with a peak at 1–2 min that declined to a mean concentration of 0.00046% ± 0.00007% of the injected dose (% AA)/mL within 5 min postdose. Metabolism was assessed by HPLC in 6 subjects, and polar metabolites with retention times at 2 and 10 min were found, whereas parent LMI1195 eluted out at 15 min. In 5 of 6 subjects, metabolism was rapid, with parent fractions of 36.5% ± 19.1%, 12.5% ± 4.3%, and 7.2% ± 2.4% at 15, 30, and 120 min after injection, respectively. The sixth subject had substantially higher parent fraction (about 2-fold), suggesting possible heterogeneity in metabolic activity. The mean ± SD urinary excretion of ^{18}F radioactivity from urine sampling for all subjects, extrapolated to infinity, was 25.2 ± 10.8% AA.

TABLE 1
τ (Hours) in Organs for ^{18}F (n = 12)

Organ	Mean	SD	Minimum	Maximum
Small intestine	0.185	0.041	0.118	0.246
Stomach wall	0.024	0.013	0.012	0.061
Heart wall	0.038	0.008	0.029	0.058
Kidneys	0.125	0.023	0.090	0.160
Liver	0.270	0.087	0.161	0.469
Lungs	0.141	0.031	0.090	0.202
Red marrow	0.159	0.032	0.100	0.221
Salivary	0.015	0.006	0.009	0.032
Spleen	0.022	0.008	0.012	0.036
Thyroid	0.008	0.001	0.005	0.010
Urinary bladder	0.199	0.043	0.083	0.250
Remainder of body	1.077	0.170	0.951	1.479

TABLE 2
Estimated Absorbed Dose in mSv/MBq (n = 12)

Organ dose	Mean	SD	Minimum	Maximum
Adrenals	0.0138	0.0009	0.0121	0.0152
Brain	0.0052	0.0007	0.0046	0.0069
Breasts	0.0065	0.0006	0.0060	0.0079
Gallbladder wall	0.0159	0.0014	0.0136	0.0187
Lower large intestine wall	0.0128	0.0007	0.0112	0.0137
Small intestine	0.0460	0.0079	0.0327	0.0581
Stomach wall	0.0308	0.0077	0.0238	0.0520
Upper large intestine wall	0.0159	0.0013	0.0136	0.0178
Heart wall	0.0285	0.0043	0.0223	0.0395
Kidneys	0.0834	0.0141	0.0608	0.1046
Liver	0.0382	0.0104	0.0249	0.0619
Lungs	0.0291	0.0053	0.0201	0.0395
Muscle	0.0081	0.0005	0.0077	0.0095
Ovaries	0.0143	0.0009	0.0123	0.0155
Pancreas	0.0136	0.0009	0.0120	0.0155
Red marrow	0.0196	0.0023	0.0150	0.0242
Osteogenic cells	0.0163	0.0015	0.0133	0.0187
Salivary glands	0.0343	0.0144	0.0204	0.0758
Skin	0.0055	0.0005	0.0051	0.0068
Spleen	0.0300	0.0080	0.0195	0.0446
Testes	0.0074	0.0005	0.0067	0.0085
Thymus	0.0080	0.0007	0.0074	0.0098
Thyroid	0.0657	0.0106	0.0465	0.0795
Urinary bladder wall	0.1015	0.0197	0.0484	0.1251
Uterus	0.0169	0.0009	0.0155	0.0183
Total body	0.0104	0.0004	0.0098	0.0115

Dosimetry

The τ for ^{18}F radioactivity in all critical organs for all 12 volunteers are summarized in Table 1. The longest τ was for the remainder tissue (1.1 h), followed by the liver (0.27 h) and urinary bladder (0.20 h). Therefore, on average, the urinary bladder wall received the largest absorbed dose, at 0.10 mSv/MBq (0.38 rem/mCi), followed by the kidneys at 0.083 mSv/MBq (0.31 rem/mCi). The mean ED was 0.026 mSv/MBq (0.096 rem/mCi).

The estimated absorbed dose for each critical organ for all 12 volunteers is summarized in Table 2. The injection of 370 MBq

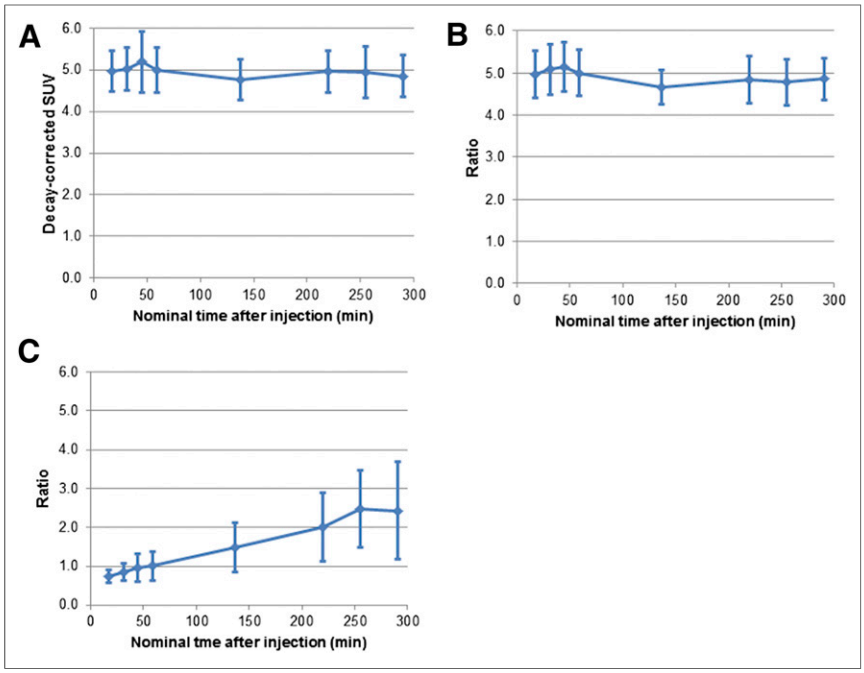

FIGURE 3. LMI1195 demonstrated favorable kinetics for cardiac imaging. Myocardial activity remained stable over 5 h (A), with favorable heart-to-lung (B) and heart-to-liver ratios (C) over same period. Error bars represent SD.

(10 mCi) of LMI1195 would result in an ED of 9.6 mSv (0.96 rem) and a dose to the urinary bladder of 38 mSv (3.8 rem). The mean ED was 0.026 mSv/MBq (0.096 rem/mCi).

Imaging Characteristics

On the basis of analyses of the mean regional SUV in the dynamic PET images, myocardial LMI1195 activity remained stable over 5 h (Fig. 3A), with favorable heart-to-lung (Fig. 3B) and heart-to-liver ratios (Fig. 3C) over the same period of time.

We applied quantitative circumferential analysis to serial reoriented cardiac images to define the regional variation of LMI1195 myocardial uptake (Fig. 4) in a subset of patients ($n = 6$). There was no significant variation ($P = 0.95$, ANOVA) in regional myocardial SUV around the circumference of the heart (anterior, 4.0 ± 0.6; septum, 3.9 ± 0.7; inferior, 3.9 ± 0.4; lateral, 3.9 ± 0.6) at 1 h after injection. There was also no significant ($P = 0.4$, ANOVA) base-to-apex gradient in myocardial uptake (base, 3.8 ± 0.7; mid ventricle, 4.0 ± 0.5; apex, 3.9 ± 0.5). These data are summarized in Figure 5.

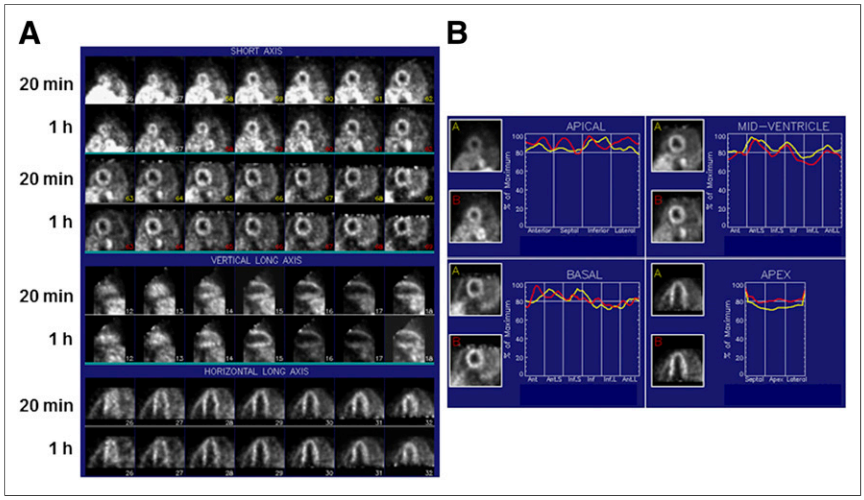

FIGURE 4. (A) Reoriented LMI1195 cardiac images in healthy volunteer at 20 min and 1 h after radiotracer injection. Shown are short-axis, vertical long-axis, and horizontal long-axis images in standard format. (B) Corresponding circumferential quantitative profiles obtained in same patient using WLCQ are shown.

DISCUSSION

Cardiac sympathetic imaging provides a noninvasive approach to risk-stratify patients with HF. This phase 1, multicenter, nonrandomized, single-dose, open-label, first-in-human clinical trial of LMI1195, a new PET imaging agent for the noninvasive assessment of sympathetic activity, demonstrates no safety concerns, rapid blood clearance, and extraction by the heart with stable myocardial activity over 5 h and a favorable biodistribution for cardiac imaging over the same period of time. Dosimetry analyses found that the urinary bladder wall receives the largest absorbed dose (0.10 mSv/MBq), followed by the kidneys (0.083 mSv/MBq). The mean ED of LMI1195 was 0.026 ± 0.001 mSv/MBq, which is similar to that reported for ^{123}I-MIBG (0.013 mSv/MBq) (*26*). Liver uptake peaked at approximately 17 min after injection and did not seem to impair visualization of myocardial uptake that reached a plateau early after injection.

LMI1195 has a fundamental chemical structure similar to ^{123}I-MIBG and demonstrates high specificity for presynaptic uptake 1 comparable to ^{123}I-MIBG (*27*). However, in preclinical studies, LMI1195 demonstrated improved imaging characteristics over ^{123}I-MIBG, with a more favorable heart-to-liver ratio in rodents and nonhuman primates. Kinetics studies in rabbits and nonhuman primates with LMI1195 suggest that the rate of myocardial uptake of this agent may be limited, more by neuronal function than by flow (*27*). Similar to ^{123}I-MIBG, LMI1195 is not a substrate for monoamine oxidase and therefore enters the cytosol and becomes trapped in neuronal vesicles (*28*).

Imaging with ^{123}I-MIBG has been the most widely used radiotracer approach for evaluation of sympathetic activity in the heart. Despite the availability of this radiotracer for more than 3 decades, widespread application of ^{123}I-MIBG imaging has been limited by suboptimal target-to-background activity and reliance on planar imaging for quantitation of myocardial activity relative to background mediastinal activity or myocardial washout. True quantification of absolute regional or global myocardial uptake

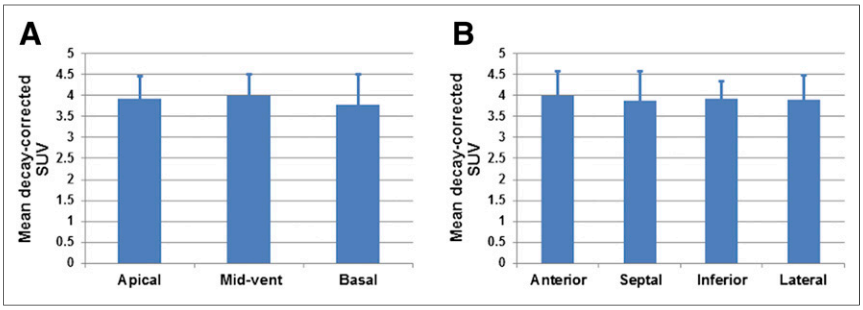

FIGURE 5. Variation in regional myocardial SUV (mean ± SD) at 1 h after injection in healthy volunteers (n = 6). Reconstructed short-axis images were interpolated into apical, mid-ventricular, and basal slices (A), and each slice was divided into anterior, septal, inferior, and lateral sectors (B) for evaluation of regional SUV. Uptake of LMI1195 was uniform in this subset of healthy volunteers. P = not significant, ANOVA.

has been limited. Although recent studies have proposed quantitative SPECT approaches (*29*), large clinical trials continue to rely on quantification from planar images (*11*).

Although PET imaging offers advantages over SPECT imaging for quantification of regional and global myocardial activity, PET sympathetic imaging agents have been principally ^{11}C-labeled, limiting widespread clinical translation of this approach. The availability of an ^{18}F-labeled sympathetic agent such as LMI1195 could open the door for large multicenter PET-based imaging trials of sympathetic activation in the setting of infarction or congestive HF for prediction of SCD. To define the true advantage of LMI1195 imaging over ^{123}I-MIBG imaging, additional head-to-head comparison studies would be required that optimize cardiac imaging with both agents.

CONCLUSION

Clinical imaging with LMI1195 appears to be feasible for the assessment of regional myocardial sympathetic activity at a time range of 10–20 min after injection of approximately 370 MBq (~10 mCi) of LMI1195. The critical organ was found to be the urinary bladder wall, with an estimated radiation dose of 0.10 ± 0.02 mSv/MBq. The estimated ED equivalent (*20*) was 0.031 ± 0.002 mSv/MBq, whereas the ED (*21*) was found to be 0.026 mSv/MBq, similar to that previously reported for ^{123}I-MIBG (*26*). These early data suggest that LMI1195 is well tolerated and yields a radiation dose comparable to that of other commonly used PET radiopharmaceuticals. Myocardial uptake and adjacent organ activity suggest that good images should be possible with acceptable patient radiation dose. This study establishes the normal pattern of quantitative regional myocardial uptake of LMI1195, which was uniform throughout the heart in healthy volunteers. LMI1195 PET imaging provides a potentially quantitative approach for evaluation of both regional denervation and the heterogeneity of innervation, indices that are likely to be predictive of SCD. This type of regional myocardial analysis may offer advantages over evaluation of heart-to-mediastinal ratios in future studies of patients with heart disease.

DISCLOSURE

The costs of publication of this article were defrayed in part by the payment of page charges. Therefore, and solely to indicate this fact, this article is hereby marked "advertisement" in accordance with 18 USC section 1734. This study was supported by a grant from Lantheus Medical Imaging. Joel Lazewatsky, PhD, Paul Crane, PhD, and L. Veronica Lee, MD, were employees of Lantheus Medical Imaging during the execution of this study. No other potential conflict of interest relevant to this article was reported.

ACKNOWLEDGMENTS

We gratefully acknowledge the technical assistance of Tim Mulnix, PhD, Donna McMahon, Maria Corsi, and the staff of the Yale PET Center.

REFERENCES

1. Jessup M, Abraham WT, Casey DE, et al. 2009 focused update: ACCF/AHA guidelines for the diagnosis and management of heart failure in adults—a report of the American College of Cardiology Foundation/American Heart Association Task Force on Practice Guidelines: developed in collaboration with the International Society for Heart and Lung Transplantation. *Circulation.* 2009;119:1977–2016.
2. Rosamond W, Flegal K, Furie K, et al. Heart disease and stroke statistics: 2008 update—a report from the American Heart Association Statistics Committee and Stroke Statistics Subcommittee. *Circulation.* 2008;117: e25–e146.
3. Rundqvist B, Elam M, Bergmann-Sverrisdottir Y, Eisenhofer G, Friberg P. Increased cardiac adrenergic drive precedes generalized sympathetic activation in human heart failure. *Circulation.* 1997;95:169–175.
4. Eisenhofer G, Friberg P, Rundqvist B, et al. Cardiac sympathetic nerve function in congestive heart failure. *Circulation.* 1996;93:1667–1676.
5. Beau SL, Saffitz JE. Transmural heterogeneity of norepinephrine uptake in failing human hearts. *J Am Coll Cardiol.* 1994;23:579–585.
6. Böhm M, La Rosee K, Schwinger RH, Erdmann E. Evidence for reduction of norepinephrine uptake sites in the failing human heart. *J Am Coll Cardiol.* 1995;25:146–153.
7. Brush JE Jr, Eisenhofer G, Garty M, et al. Cardiac norepinephrine kinetics in hypertrophic cardiomyopathy. *Circulation.* 1989;79:836–844.
8. Carrió I, Cowie MR, Yamazaki J, Udelson J, Camici PG. Cardiac sympathetic imaging with mIBG in heart failure. *JACC Cardiovasc Imaging.* 2010;3:92–100.
9. Higuchi T, Schwaiger M. Noninvasive imaging of heart failure: neuronal dysfunction and risk stratification. *Heart Fail Clin.* 2006;2:193–204.
10. Tobes MC, Jaques S Jr, Wieland DM, Sisson JC. Effect of uptake-one inhibitors on the uptake of norepinephrine and metaiodobenzylguanidine. *J Nucl Med.* 1985;26:897–907.
11. Jacobson AF, Senior R, Cerqueira MD, et al. Myocardial iodine-123 meta-iodobenzylguanidine imaging and cardiac events in heart failure: results of the prospective ADMIRE-HF (AdreView Myocardial Imaging for Risk Evaluation in Heart Failure) study. *J Am Coll Cardiol.* 2010;55: 2212–2221.
12. Katoh S, Shishido T, Kutsuzawa D, et al. Iodine-123-metaiodobenzylguanidine imaging can predict future cardiac events in heart failure patients with preserved ejection fraction. *Ann Nucl Med.* 2010;24:679–686.
13. Tamaki S, Yamada T, Okuyama Y, et al. Cardiac iodine-123 metaiodobenzylguanidine imaging predicts sudden cardiac death independently of left ventricular ejection fraction in patients with chronic heart failure and left ventricular systolic dysfunction: results from a comparative study with signal-averaged electrocardiogram, heart rate variability, and QT dispersion. *J Am Coll Cardiol.* 2009;53:426–435.
14. Fallavollita JA, Heavey BM, Luisi AJ Jr, et al. Regional myocardial sympathetic denervation predicts the risk of sudden cardiac arrest in ischemic cardiomyopathy. *J Am Coll Cardiol.* 2014;63:141–149.
15. Yu M, Bozek J, Lamoy M, et al. Evaluation of LMI1195, a novel ^{18}F-labeled cardiac neuronal PET imaging agent, in cells and animal models. *Circ Cardiovasc Imaging.* 2011;4:435–443.

16. Hilton J, Yokoi F, Dannals RF, Ravert HT, Szabo Z, Wong DF. Column-switching HPLC for the analysis of plasma in PET imaging studies. *Nucl Med Biol.* 2000; 27:627–630.
17. Siegel JA, Thomas SR, Stubbs JB, et al. MIRD pamphlet no. 16: techniques for quantitative radiopharmaceutical biodistribution data acquisition and analysis for use in human radiation dose estimates. *J Nucl Med.* 1999;40: 37S–61S.
18. Stabin MG, Sparks RB, Crowe E. OLINDA/EXM: the second-generation personal computer software for internal dose assessment in nuclear medicine. *J Nucl Med.* 2005;46:1023–1027.
19. Food and Drug Administration. *Guidance for Industry: Developing Medical Imaging Drug and Biological Products—Part 1: Conducting Safety Assessments.* FDA.gov. http://www.fda.gov/downloads/Drugs/GuidanceComplianceRegulatoryInformation/Guidance/ucm078930.pdf. June 2004. Accessed June 24, 2014.
20. International Commission on Radiological Protection (ICRP). *Recommendations of the International Commission on Radiological Protection.* ICRP publication 26. Oxford, U.K.: Pergamon Press; 1977.
21. International Commission on Radiological Protection (ICRP). *1990 Recommendations of the International Commission on Radiological Protection*. ICRP publication 60. Oxford, U.K.: Pergamon Press; 1991.
22. International Commission on Radiological Protection (ICRP). *Basic Anatomical and Physiological Data for use in Radiological Protection: The Skeleton*. ICRP publication 70. Oxford, U.K.: Pergamon Press; 1994.
23. International Commission on Radiological Protection (ICRP). *Report of the Task Group on Reference Man.* ICRP publication 23. Oxford, U.K.: Pergamon Press; 1975.
24. Loevinger RBT, Watson EE. *MIRD Primer for Absorbed Dose Calculations*. New York, NY: Society of Nuclear Medicine; 1991.
25. Loening AM, Gambhir S. AMIDE: a free software tool for multimodality medical image analysis. *Mol Imaging.* 2003;2:131–137.
26. International Commission on Radiological Protection (ICRP). *Radiation Dose to Patients from Radiopharmaceuticals (Addendum 2 to ICRP Publication 53)*. ICRP publication 80. Oxford, U.K.: Pergamon Press; 1999.
27. Yu M, Bozek J, Lamoy M, et al. LMI1195 PET imaging in evaluation of regional cardiac sympathetic denervation and its potential role in antiarrhythmic drug treatment. *Eur J Nucl Med Mol Imaging.* 2012;39:1910–1919.
28. Thackeray JT, Bengel FM. Assessment of cardiac autonomic neuronal function using PET imaging. *J Nucl Cardiol.* 2013;20:150–165.
29. Chen J, Folks RD, Verdes L, Manatunga DN, Jacobson AF, Garcia EV. Quantitative I-123 mIBG SPECT in differentiating abnormal and normal mIBG myocardial uptake. *J Nucl Cardiol.* 2012;19:92–99.